Journal Name

ARTICLE

Polynuclear Ampyrone based 3d Coordination Clusters

Stavroula I. Sampani,[a] Edward Loukopoulos,[a] Mohammad Azam,[a,b] Kieran Griffiths,[a] Alaa Abdul-Sada,[a] Graham Tizzard,[c] Simon Coles,[c] Albert Escuer,*[d] Athanassios Tsipis*[e] and George E. Kostakis*[a]

Received 00th January 20xx,
Accepted 00th January 20xx

DOI: 10.1039/x0xx00000x

www.rsc.org/

The use of the monoanionic Schiff base ligand (E)-4-(2-hydroxybenzylideneamino)-2,3-dimethyl-1-phenyl-1,2-dihydropyrazol-5-one in transition (Co, Ni and Cu) coordination chemistry yields mono-, tetra- and pentanuclear Coordination Clusters with different structural motifs. An organic transformation occurs in the ligand in the Cu compound for which theoretical studies are presented. Solution studies, topological issues and magnetic studies are discussed. The present results demonstrate the richness of the coordination chemistry of this monoprotic organic ligand, which promotes the formation of high-nuclearity CCs.

Introduction

The coordination chemistry of polynuclear transition metal coordination clusters (CCs),[1] assembled by organic or inorganic ligands, has received considerable attention today. These materials find applications in biological systems,[2,3] magnetism,[4–9] material science,[10–15] photochemistry[16,17] and as components in catalytic procedures.[18–20] The synthesis of such finite molecules is mainly based on serendipity,[21] however the employment of an organic ligand, that bears numerous coordination sites, facilitates their synthesis. Schiff base ligands are of particular interest due to their ease of synthesis and multiple coordination sites, thus have been extensively used for the synthesis of polynuclear CCs.[22–28]

Ampyrone, also known as 4-aminoantipyrine, is a pyrazole derivative that has a keto group at position 5 and is substituted at position 4 by an amino group (**A**, Scheme 1). This organic scaffold has been used for the synthesis of dihydrotestosterone products,[29] whilst its derivatives, exhibit cycotoxic,[30] antimicrobial[31] or anagesic[32] activity, similar bioactivity to ampicillin and streptomycin,[33] and has been used to produce redox active Ru CCs,[34] hydrogen bonded frameworks,[35] fluorescent chemo sensors for F^{-}[36] and Cu^{2+}/F^{-}[37] recognition, selective probes for Al^{3+} and cysteine detection,[38] and pigments.[39] Additionally, due to the presence of the amino and keto groups ampyrone can react with another organic scaffold that bears an aldehyde/ketone or amino group, yielding Schiff base ligands with multiple donor sites, which in turn can be excellent candidates for the construction of polynuclear CCs.

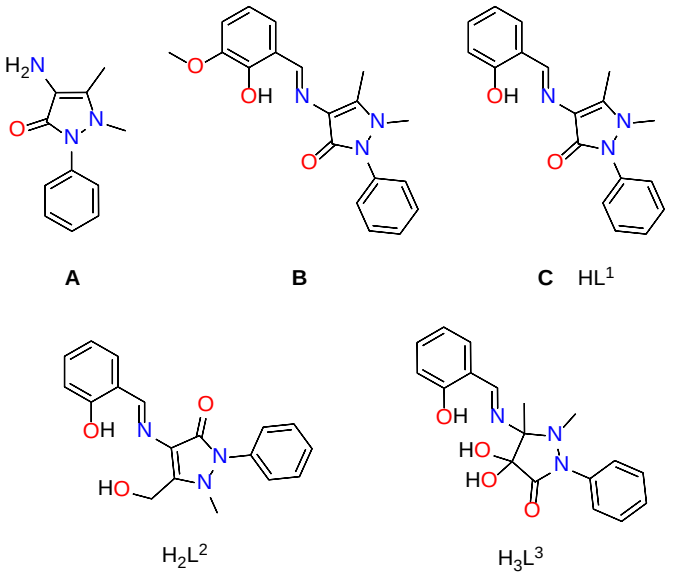

Scheme 1. (Upper) Ampyrone (**A**) and its derivatives **B** and **C**, (this study) used for the synthesis of polynuclear CCs.(Lower) The protonated form of the transformed ligands H_2L^2 and H_3L^3.

We recently initiated a project towards the synthesis of homo- and heterometallic polynuclear CCs with the use of the ligand (E)-4-(2-hydroxy-3-methoxybenzylideneamino)-2,3-dimethyl-1-phenyl-1,2-dihydropyrazol-5-one (**B**, Scheme 1) that is a Schiff base ligand produced from the condensation of o-vanillin and ampyrone. The employment of **B** in 3d and 4f chemistry yielded a series of polynuclear CCs displaying previously unseen topologies, interesting magnetic properties and unexpected chemical transformations.[40–43] According to a detailed literature survey,[44] the organic ligand **C** (HL^1, Scheme

[a] *Department of Chemistry, School of Life Sciences, University of Sussex, Brighton BN19QJ, UK, E-mail: G.Kostakis@sussex.ac.uk*
[b] *Department of Chemistry, College of Sciences, King Saud University, P.O. Box: 2455, Riyadh 11451, KSA.*
[c] *UK National Crystallography Service, Chemistry, University of Southampton, SO171BJ, UK.*
[d] *Departament de Química Inorgànica i Orgànica, Secció Inorgànica and Institut de Nanociència i Nanotecnologia (IN2UB), Universitat de Barcelona, Martí i Franques 1-11, Barcelona-08028, Spain. E-mail: albert.escuer@qi.ub.es*
[e] *Laboratory of Inorganic and General Chemistry, Department of Chemistry, University of Ioannina, 451 10 Ioannina, Greece. E-mail: attsipis@uoi.gr*
Electronic Supplementary Information (ESI) available: [Crystallographic Tables, Figures of compounds, H-bonding Tables, NMR and ESI characterization]. See DOI: 10.1039/x0xx00000x

Please do not adjust margins

1) that is structural related to **B**, lacking a methoxy group, and its derivatives have been used for the synthesis of low nuclearity compounds such as the mononuclear Ni,[35] Co,[35] Cu,[45,46] and Re[47] and dinuclear Co_2[48] and Cu_2[49] species. Therefore, as an extension of our previous study, we envisioned that HL^1 can yield polynuclear CCs and therefore in this work, we used this specific unit as template to yield coordination compounds of high nuclearities. We report herein the use of HL^1 in Co^{II}, Ni^{II} and Cu^{II} chemistry and thus present the synthesis, characterization and crystal structure of nine CCs formulated as $[Ni(L^1)_2]\cdot 3MeCN$ (**2**), $[Co(L^1)_2]\cdot 3MeCN$ (**1**), $[Cu(L^1)(piv)]\cdot H_2O$ (**3**), $[Cu(L^1)(1\text{-nap})]_2ClO_4\cdot H_2O\cdot[Et_3NH]^+$ (**4**), $[Ni_2(L^1)_2(4\text{-nba})(H_2O)(EtOH)]\cdot ClO_4$ (**5**), $[Ni_4(\mu_3\text{-}OH)(L^1)_4(EtOH)_2]\cdot 2ClO_4\cdot 5EtOH$ (**6**), $[Ni_4(L^1)_4(piv)_2]\cdot 2ClO_4\cdot 2MeCN\cdot(H_2O)$ (**7**), $[Ni_5(\mu_2\text{-}OH)(\mu_3\text{-}OCH_3)_2(L^1)_5(H_2O)]\cdot 2ClO_4\cdot 4DMF$ (**8**) and $[Cu_4(L^2)_4(L^3)_4]\cdot 3MeCN$ (**9**), (where piv = pivalic acid, 1-nap = 1-napthoic acid, 4-nba = 4-nitrobenzoic acid) as well as the magnetic properties for representative compounds **6**-**9**. Synthetic and topological issues are discussed. In addition, we report interesting case of ligand transformation found in **9** supported by theoretical density functional theory studies.

Experimental Section

Materials. Chemicals (reagent grade) were purchased from Sigma Aldrich, Acros Organics and Alfa Aesar. All experiments were performed under aerobic conditions using materials and solvents as received. *Safety note*: Perchlorate salts are potentially explosive; such compounds should be used in small quantities and handled with caution and utmost care at all times.

Instrumentation. IR spectra of the samples were recorded over the range of 4000-650 cm^{-1} on a Perkin Elmer Spectrum One FT-IR spectrometer fitted with a UATR polarization accessory. EI-MS was performed on a VG Autospec Fissions instrument (EI at 70 eV). NMR spectra were measured on a Varian VNMRS solution-state spectrometer at 500 MHz at 30°C. Chemical shifts are quoted in parts per million (ppm). Coupling constants (J) are recorded in Hertz (Hz). Elemental analysis data were recorded at Science Centre, London Metropolitan University, 29 Hornsey Road, London N7 7DD, UK.

Magnetic studies. Magnetic susceptibility measurements were carried out on polycrystalline samples with a MPMS5 Quantum Design susceptometer working in the range 30-300 K under external magnetic field of 0.3 T and under a weaker field of 0.03T in the 30 – 2 K range to avoid saturation effects. Diamagnetic corrections were estimated from Pascal Tables.

X-ray Crystallography. Data for HL^1 and compounds **1**, **2**, **5**, **6**, **7** and **8** were collected (ω-scans) at the University of Sussex using an Agilent Xcalibur Eos Gemini Ultra diffractometer with CCD plate detector under a flow of nitrogen gas at 173(2) K using either Mo Kα (λ = 0.71073 Å) or Cu Kα radiation (λ = 1.54184 Å). CRYSALIS CCD and RED software was used respectively for data collection and processing. Reflection intensities were corrected for absorption by the multi-scan method. Data for **3**, **4** and **9** were collected at the National Crystallography Service, University of Southampton[50]. All structures were determined using Olex2[51], solved using SHELXT[52] and refined with SHELXL-2014[53]. All non-H atoms were refined with anisotropic thermal parameters, and H-atoms were introduced at calculated positions and allowed to ride on their carrier atoms. Crystal data and structure refinement parameters for all compounds are given in Tables S1 and S2. Geometric/crystallographic calculations were performed using PLATON[54], Olex2[51], and WINGX[55] packages; graphics were prepared with Crystal Maker and MERCURY[56]. Each of the crystal structures has been deposited at the CCDC 1588912-1588921.

Synthetic part

Synthesis of HL^1. Equivalent amounts of salicylaldehyde and 4-aminoantipyrine were refluxed in methanolic solution for 2 hours. The ligand was obtained after filtration in 95% yield, washed with cold methanol, then washed with Et_2O and dried in air. Re-crystallization in EtOH produced large yellow block crystals. ^{1}H NMR (500 MHz, $CDCl_3$) δ 13.34 (s, 1H), 9.84 (s, 1H), 7.52 – 7.27 (m, 7H), 6.95 (d, *J* = 8.2 Hz, 1H), 6.92 – 6.87 (m, 1H), 3.16 (s, 3H), 2.40 (s, 3H). ^{13}C NMR (126 MHz, $CDCl_3$) δ 160.62, 160.47, 160.26, 149.85, 134.36, 131.95, 131.83, 129.28, 127.28, 124.62, 120.25, 119.07, 116.71, 116.25, 35.63, 10.24. EI: 307 [M – H]. Crystal Data for $C_{18}H_{17}N_3O_2$ (*M* =307.34 g/mol): monoclinic, space group $P2_1/n$ (no. 14), *a* = 7.4861(3) Å, *b* = 7.4773(3) Å, *c* = 27.3003(10) Å, *β* = 95.532(4)°, *V* = 1521.04(11) Å^3, *Z* = 4, *T* = 173 K, μ(CuKα) = 0.725 mm^{-1}, *Dcalc* = 1.342 g/cm^3, 4473 reflections measured (12.01° ≤ 2Θ ≤ 141.988°), 2808 unique (R_{int} = 0.0221, R_{sigma} = 0.0338) which were used in all calculations. The final R_1 was 0.0451 (I > 2σ(I)) and wR_2 was 0.1250 (all data).

Synthesis of $[Ni(L^1)_2]\cdot 3MeCN$ (1). 0.2 mmol (0.062 g) of HL^1 and 0.7 mmol (93.8 μL) of Et_3N were dissolved in 20 ml MeCN. 0.1 mmol (0.037 g) of $Ni(ClO_4)_2\cdot 6H_2O$ were then added. The resultant green solution was refluxed for 2 hours, filtered and left to evaporate slowly. Green crystals were formed after 1 day. Yield: 16% (based on Ni). Selected IR peaks (cm^{-1}): 3017 (w), 2942 (w), 1738 (m), 1608 (s), 1583 (s), 1527 (m), 1490 (m), 1472 (m), 1442 (s), 1388 (w), 1315 (m), 1204 (w), 1147 (w), 1071 (m), 1021 (m), 902 (w), 854 (w), 760 (m), 722 (m), 693 (m), 677 (m). Elemental analysis for $C_{42}H_{41}N_9NiO_4$: calcd. C 63.78, H 4.85, N 15.95, found C 63.61, H 4.81, N 15.77.

Synthesis of $[Co(L^1)_2]\cdot 3MeCN$ (2). 0.2 mmol (0.062 g) of HL^1 and 0.7 mmol (93.8 μL) of Et_3N were dissolved in 20 ml MeCN. 0.1 mmol (0.037 g) of $Co(ClO_4)_2\cdot 6H_2O$ were then added. The resultant orange solution was refluxed for 2 hours, filtered and left to evaporate slowly. Brown crystals were formed after 1 day. Yield: 21% (based on Co). Selected IR peaks (cm^{-1}): 3030 (w), 2948 (w), 1740 (m), 1609 (s), 1582 (s), 1516 (m), 1490 (m), 1470 (m), 1439 (s), 1381 (w), 1310 (m), 1204 (w), 1145 (w), 1075 (m), 1021 (m), 902 (w), 852 (w), 758 (m), 720 (m), 692 (m), 671 (m). Elemental analysis for $C_{42}H_{41}N_9CoO_4$: calcd. C 63.46, H 5.20, N 15.87, found C 63.29, H 5.16, N 15.70.

Synthesis of $[Cu(L^1)(piv)]\cdot H_2O$ (3). 0.2 mmol (0.062 g) of HL^1 and 0.7 mmol (93.8 μL) of Et_3N were dissolved in 20 ml MeCN. 0.1 mmol (0.037 g) of $Cu(ClO_4)_2\cdot 6H_2O$ were then added and stirred for 5 min. Then 0.5 mmol (0.052 mg) of pivalic acid were added

into the mixture. The resultant green solution was refluxed for 2 hours, filtered and left to evaporate slowly Brown crystals were formed after 2 weeks. Yield: 18% (based on Cu). Selected IR peaks (cm^{-1}): 3057 (w), 1656 (m), 1604 (s), 1578 (m), 1523 (m), 1495 (m), 1456 (m), 1432 (m), 1386 (m), 1348 (w), 1292 (m), 1240 (w), 1196 (w), 1137 (m), 1026 (m), 968 (w), 911 (w), 856 (w), 746 (s), 713 (m), 692 (s), 679 (m). Elemental analysis for $C_{23}H_{27}N_3CuO_5$: calcd. C 56.54, H 5.57, N 8.61, found C 56.42, H 5.67, N 8.80.

Synthesis of $[Cu(L^1)(1\text{-nap})]_2{\cdot}ClO_4{\cdot}H_2O{\cdot}[Et_3NH]^+$ (4). **4** was prepared in the same method as **3**, with 1-naphthoic acid as the co-ligand. Brown crystals were formed after 4 days. Yield: 14% (based on Cu). Selected IR peaks (cm^{-1}): 3044 (w), 1607 (s), 1564 (m), 1532 (m), 1498 (m), 1462 (w), 1399 (w), 1367 (m), 1328 (m), 1255 (w), 1193 (w), 1150 (w), 1024 (m), 970 (w), 871 (w), 793 (m), 782 (m), 759 (s), 731 (m), 678 (m), 660 (m). Elemental analysis for $C_{35}H_{41}N_4Cl_2CuO_{13}$: calcd. C 48.94, H 4.82, N 6.53, found C 48.79, H 4.91, N 6.63.

Synthesis of $[Ni_2(L^1)_2(4\text{-nba})(H_2O)(EtOH)]{\cdot}ClO_4$ (5). **5** was prepared in a similar fashion to **1**, with the addition of 4-nitrobenzoic acid (0.5 mmol, 0.084 g) into the mixture. Yellow crystals were obtained after 3 days. Yield: 11% (based on Ni). Selected IR peaks (cm^{-1}): 3014 (w), 2971 (w), 1739 (s), 1600 (m), 1587 (m), 1520 (w), 1443 (m), 1366 (s), 1309 (w), 1217 (s), 1093 (m), 900 (w), 762 (m), 722 (m), 695 (m), 675 (m). Elemental analysis for $C_{45}H_{44}N_7ClNi_2O_{14}$: calcd. C 51.08, H 4.19, N 9.27, found C 51.15, H 4.19, N 9.21.

Synthesis of $[Ni_4(\mu_3\text{-}OH)(L^1)_4(EtOH)_2]{\cdot}2ClO_4{\cdot}5EtOH$ (6). 0.1 mmol (0.031 g) of HL^1 and 0.6 mmol (80.4 µL) of Et_3N were dissolved in 20 ml EtOH. 0.1 mmol (0.037 g) of $Ni(ClO_4)_2{\cdot}6H_2O$ were then added. The resultant green solution was refluxed for 2 hours, filtered and left to evaporate slowly. Green crystals were formed after 2 weeks. Yield: 21% (based on Ni). Selected IR peaks (cm^{-1}): 3027 (w), 2971 (w), 1738 (s), 1603 (s), 1571 (m), 1533 (m), 1491 (w), 1444 (m), 1390 (m), 1269 (m), 1090 (s), 900 (w), 808 (w), 760 (s), 723 (m), 692 (m), 676 (m). Elemental analysis for $C_{86}H_{108}N_{12}Cl_2Ni_4O_{25}$: calcd. C 51.33, H 5.41, N 8.36, found C 51.28, H 5.29, N 8.32.

Synthesis of $[Ni_4(L^1)_4(piv)_2]{\cdot}2ClO_4{\cdot}2MeCN{\cdot}(H_2O)$ (7). **7** was prepared in the same method as **1**, with the addition of 0.5 mmol (0.052 mg) of pivalic acid into the mixture. Green crystals were formed after 1 week. Yield: 12% (based on Ni). Selected IR peaks (cm^{-1}): 3023 (w), 2971 (w), 1738 (s), 1603 (s), 1583 (s), 1525 (m), 1490 (m), 1442 (m), 1375 (s), 1217 (m), 1176 (m), 1094 (m), 901 (w), 854 (w), 807 (w), 760 (s), 722 (m), 693 (m), 677 (m). Elemental analysis for $C_{86}H_{90}Cl_2N_{14}Ni_4O_{21}$: calcd. C 52.67, H 4.62, N 10.00, found C 52.55, H 4.69, N 9.91.

Synthesis of $[Ni_5(\mu_2\text{-}OH)(\mu_3\text{-}OCH_3)_2(L^1)_5(H_2O)]{\cdot}2ClO_4{\cdot}4DMF$ (8). 0.25 mmol (0.095 g) of HL^1 and 1 mmol (139 µL) of Et_3N were dissolved in MeOH and 0.25 mmol (0.092 g) of $Ni(ClO_4)_2{\cdot}6H_2O$ were then added. The resultant green solution was refluxed for 5 hours and filtered after cooling down. The obtained green precipitate was then dissolved in DMF and subjected to vapor diffusion of diethyl ether. Green crystals were formed after 5 days. Yield: 19% (based on Ni). Selected IR peaks (cm^{-1}): 2928 (w), 1663 (m), 1607 (s), 1580 (m), 1540 (w), 1492 (w), 1472 (m), 1458 (m), 1441 (m), 1314 (m), 1254 (w), 1153 (w), 1084 (s), 906 (w), 761 (m), 694 (m), 622 (m). Elemental analysis for $C_{211}H_{237}Cl_4N_{39}Ni_{10}O_{51}$: calcd. C 52.11, H 4.91, N 11.23, found C 51.99, H 5.02, N 11.17.

Synthesis of $[Cu_4(L^2)_4(L^3)_4]{\cdot}3MeCN$ (9). The synthetic procedure of **3** also generated green crystals within 1 day, the structure of which was determined as of compound **9**. Yield: 49% (based on Cu). Selected IR peaks (cm^{-1}): 3031 (w), 2971 (w), 1738 (s), 1610 (m), 1560 (m), 1478 (m), 1435 (m), 1401 (m), 1370 (s), 1217 (s), 1158 (w), 1106 (m), 965 (w), 884 (m), 854 (m), 761 (m), 725 (m), 697 (m), 675 (m). Elemental analysis for $C_{78}H_{73}N_{15}Cu_4O_{14}$: calcd. C 55.21, H 4.34, N 12.39, found C 55.29, H 4.32, N 12.48.

Results and Discussion

Mononuclear compounds **1** and **2** are isostructural, therefore only **1** will be described in detail. The complex crystallises in the P-1 triclinic space group. Its asymmetric unit contains one Ni^{II} ion, two deprotonated organic ligands (L^1) and three lattice acetonitrile molecules (Figure 1). Both organic ligands demonstrate the same coordination mode (Scheme 2-I), fulfilling the Ni^{II} ions coordination geometry with a (N_2O_4) donor set. The Ni^{II} ions coordination geometry can be described as distorted octahedral and Ni-O bond lengths range between 2.002(13) - 2.204(12) Å. No supramolecular interactions (H-bonds, stacking) can be found between neighbouring entities.

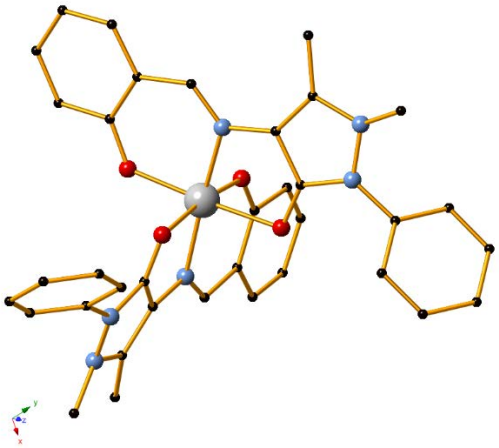

Figure 1. The structure of compounds **1** and **2** (X = Ni and Co). H atoms and lattice solvent molecules are omitted for clarity. Colour code X (grey), O (red), C (black), N (blue).

Compound **3** crystallises in the triclinic P-1 space group. The co-ligand pivalic acid was employed during preparation to enhance variation in the resulting structure. As such, the mononuclear formed complex contains a Cu^{II} ion, one deprotonated L^1 molecule, one deprotonated co-ligand molecule and a lattice water molecule in the asymmetric unit (Figure S2). The L^1 ligand exhibits the same coordination mode as in the case of **1** and **2**, while pivalic acid coordinates to the metal centre through one oxygen atom. As a result, Cu^{II} presents a (NO_3) coordination environment and a square planar geometry. The respective Cu-O distances range from 1.896(3) to 1.999(3) Å, while the mean Cu-N bond length was measured at 1.966(2) Å. Furthermore, the lattice water molecule in **3**

participates in two strong O-H···O hydrogen bonds (Table S6), ensuring the stability of the supramolecular architecture in the compound.

Compound **4** was synthesized through the addition of the co-ligand 1-naphtoic acid and results in a structure that is slightly different compared to **3**. In this case, the complex crystallises in the orthorhombic $P2_12_12$ space group and its asymmetric unit contains two different mononuclear [$Cu^{II}(L^1)$(1-nap)] species; a water molecule, a perchlorate anion and a protonated trimethylamine are also present in the lattice (Figure S3). While L^1 ligand exhibits the same coordination mode (Scheme 2-I) as the previously described compounds, the coordination mode of the co-ligand is different in this case, as both oxygen atoms of 1-nap coordinate to the Cu^{II} ion. As a result, the geometry of the pentacoordinated metal centre for each monomer species is trigonal bipyramidal (τ = 0.87 for Cu1, 0.92 for Cu11)[57]. The mean Cu-O and Cu-N distances range from 1.906(6) to 2.502(8) and from 1.962(6) to 1.970(7) Å, respectively. The remaining lattice components participate in a network of intramolecular strong hydrogen bonds, which stabilise the structure. These are listed in Table S8.

The dinuclear compound **5** crystallises in the P-1 triclinic space group. The asymmetric unit of **5** contains two Ni^{II} ions, two deprotonated organic ligands, one deprotonated 4-nitrobenzoic acid co-ligand (4-nba), a coordinated methanol and water molecule and a perchlorate ion (Figure 2). The Ni_2O_2 core forms a distorted square with a Ni1-Ni2 distance of 2.9457(7) Å, while Ni-O bond lengths range from 1.983(3) to 2.112(3) Å. Both L^1 ligands display the same coordination mode (Scheme 2-IV) with each phenol group bridging Ni1 and Ni2. The 4-nba co-ligand also bridges Ni1 and Ni2 (Scheme 4). The coordination geometry is fulfilled by a water molecule (for Ni1) and a methanol solvent molecule (for Ni2). As a result, both Ni^{II} ions display a distorted octahedral geometry with a (NO_5) donor set. No supramolecular interactions (H-bonds, stacking) can be found in the structure.

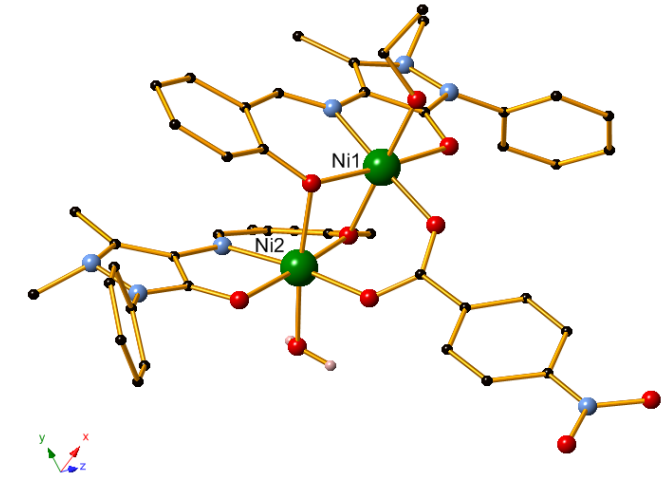

Figure 2. The structure of compound **5**. H atoms, counter ions and lattice solvent molecules are omitted for clarity. Colour code Ni (dark green), O (red), C (black), N (blue).

The tetranuclear compound **6** crystallises in the $P2_1/c$ monoclinic space group. The asymmetric unit contains four Ni^{II} ions, four deprotonated organic ligands, two triply bridging hydroxide ions, two co-ordinated ethanol molecules, two perchlorate counter ions and five lattice ethanol solvent molecules. The main core of **6** can be considered a Ni_4O_4 distorted cube with Ni^{II} ions and O nodes at alternating vertices (Figure 3). Within this cube, Ni-O bond lengths range in length between 1.969(3) - 2.216(3) Å and Ni-O-Ni bond angles between 90.55(10) - 104.52(11)°. All Ni^{II} ions display a (N_1O_5) coordination sphere and distorted octahedral geometry. L^1 ligand displays two co-ordination modes; two ligands support the Ni_4O_4 core via phenolic oxygens within the cube, these are aligned to the diagonal hydroxide ions included within the core on the same face (Scheme 2, Coordination mode II). The other two only fulfil the co-ordination environment of Ni^{II} ions (Ni02-Ni04, Ni01-Ni03) and coordinating groups are not involved in the formation of the Ni_4O_4 cube (Scheme 2, coordination mode III). Both hydroxide ions are triply bridging between Ni02-Ni03-Ni04 and Ni01-Ni03-Ni04. Multiple strong H-bonding interactions are observed within the crystal structure (Table S11), the first of these between a phenolic oxygen of L^1 and a coordinated EtOH and the second between a bridging hydroxide ion and a lattice EtOH molecule. An additional weaker hydrogen bond is observed between the aforementioned and a ClO_4 counter ion. No other supramolecular interactions can be found between neighbouring entities.

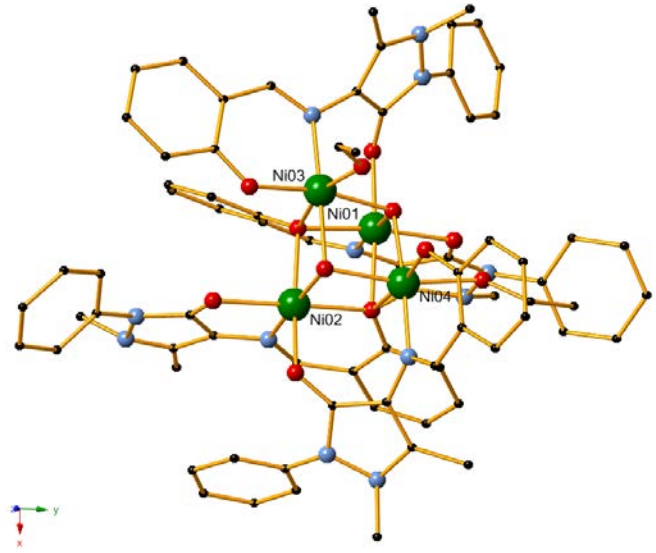

Figure 3. The crystal structure of compound **6**. H atoms, counter ions and lattice solvent molecules are omitted for clarity. Colour code Ni (dark green), O (red), C (black), N (blue).

The tetranuclear compound **7** crystallise in the P-1 triclinic space group. Its asymmetric unit contains four Ni^{II} ions, four deprotonated organic ligands, two deprotonated pivalic acid molecules, two perchlorate counter ions, one lattice water molecule and two acetonitrile solvent molecules. The main core of **7** can be consider a Ni_4O_4 distorted cube with Ni^{II} ions and O nodes at alternating vertices (Figure 4), similar in fashion to **6**. However in this compound the Ni_4O_4 cube appears less

distorted, as the range between relevant bond lengths and angles is smaller; the Ni-O bond lengths and Ni-O-Ni bond angles range between 1.999(2) and 2.1565(18) Å, and between 89.27(7) and 100.29(8)°, respectively. As in compound **6**, the phenolic oxygens of each L^1 ligand are included within the core. All Ni^{II} ions display a distorted octahedral geometry with all ligands adopting co-ordination mode II (Scheme 2). All Ni^{II} centres also possess the same donor set (N_1O_5) and the co-ordination of each ion is fulfilled via bridging pivalic acid molecules. One co-ligand bridges the Ni01 and Ni03 metal centres, while the second co-ligand bridges Ni02 and Ni04. Two strong O-H···O hydrogen bonds are also formed to further stabilize the structure. The values for these bonds may be found in Table S13.

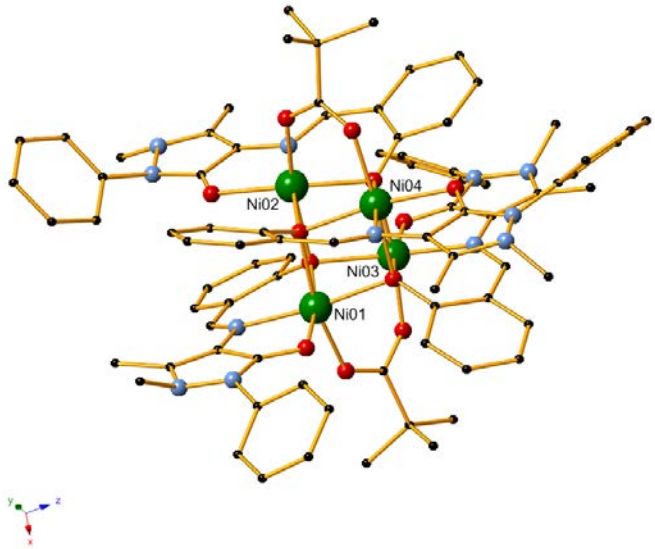

Figure 4. The crystal structure of complex **7**. H atoms, counter ions and lattice solvent molecules are omitted for clarity. Colour code Ni (dark green), O (red), C (black), N (blue).

The pentanuclear compound **8** crystallises in the $P2_1/c$ monoclinic space group. The asymmetric unit contains five Ni^{II} ions, five deprotonated organic ligands, two triply bridging methoxy groups, one triply bridging hydroxy group, four lattice solvent DMF molecules and two perchlorate counter ions. The main core of **8** can be considered as three fused triangles with a Ni^{II} cation occupying each vertice (Figure 5). As a result, Ni1, Ni3 and Ni5 occupy one plane while Ni2 and Ni4 occupy a different plane. The core can be represented as Ni_5O_8 with Ni nodes at the two apex vertices alternating with O. The eight O nodes in the core derive from coordinated phenolic oxygens and the hydroxy and methoxy bridging groups. The organic ligand L^1 demonstrates two coordination modes (Scheme 2) with two ligands displaying coordination mode IV and three ligands displaying coordination mode V. As for the bridging groups, each group bridges three Ni^{II} centres; the methoxy bridges are formed between Ni1-Ni2-Ni3 and Ni2-Ni3-Ni4 respectively, while the hydroxy group provides the third support of the core and bridges Ni-3-Ni4-Ni5. As a result, each Ni^{II} centres is six-coordinated with a (NO_5) donor set and geometry may be best described as a distorted octahedral. The Ni-O bond lengths ranging between 1.992(3) and 2.254(3) Å, while the Ni-O-Ni angles range between 95.60(14) and 100.78(13)°. Selected bond distances and angles may be found in Table S14. The stability of the structure is further increased through the formation of a strong O-H···O hydrogen bond between the hydroxy group and a lattice DMF molecule. No other supramolecular interactions can be found between neighbouring entities.

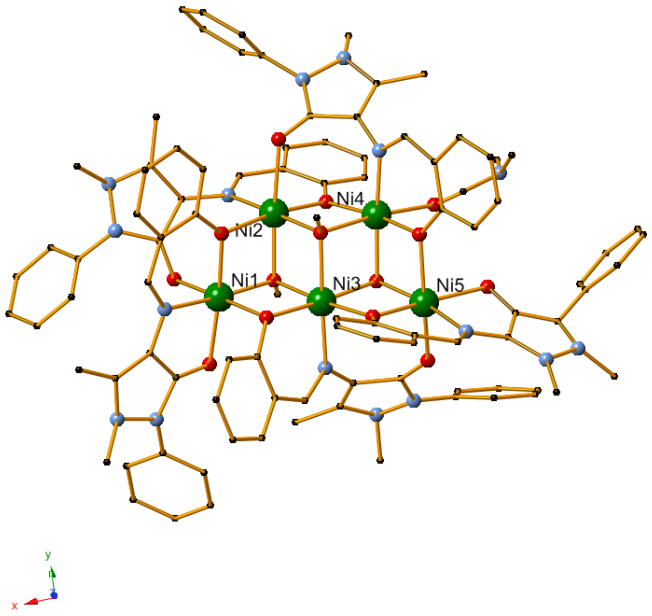

Figure 5. The crystal structure of complex **8**. H atoms, counter ions and lattice solvent molecules are omitted for clarity. Colour code Ni (dark green), O (red), C (black), N (blue).

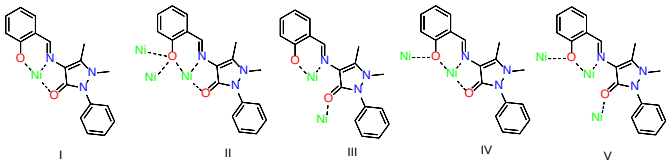

Scheme 2. Co-ordination modes displayed in compounds **2, 6, 7** and **8**

The tetranuclear compound **9** crystallises in the C2/c monoclinic space group. The asymmetric unit of **9** contains four Cu^{II} ions, two transformed doubly deprotonated organic ligands (Scheme 3, H_2L^2), two other transformed doubly deprotonated ligands (Scheme 3, H_3L^3) and four lattice MeCN solvent molecules (Figure 6). The formed Cu_4O_6 core can be considered a defected dicubane with a number of nodes unfilled, forming an empty cavity, while the Cu^{II} nodes form a horizontal lozenge along the X axis with two "body" and two "wing" positions occupying the vertices of the lozenge. The "body" Cu^{II} centres (Cu1) are six-coordinated and display a distorted octahedral geometry with a (NO_5) donor set. The "wing" Cu^{II} centres (Cu2) are five-coordinated and possess distorted trigonal bipyramidal geometry with a (NO_4) donor set. The trigonality index is 0.61[57] and confirms the distortion. The mean Cu-O bond distances range from 1.8781(12) to 2.3579(13) Å. The coordination of all Cu^{II} ions is fulfilled only via the transformed organic ligands $[L^2]^{2-}$ and $[HL^3]^{2-}$ with no solvent molecules or anions coordinating.

The transformed organic ligands each display one coordination mode (Scheme 2). Finally, a strong hydrogen bond (Table S16) is formed between the protonated hydroxyl group of $[HL^3]^{2-}$ and the deprotonated transformed hydroxy group of $[HL^3]^{2-}$. No other supramolecular interactions (H-bonds, stacking) can be found between neighbouring entities.

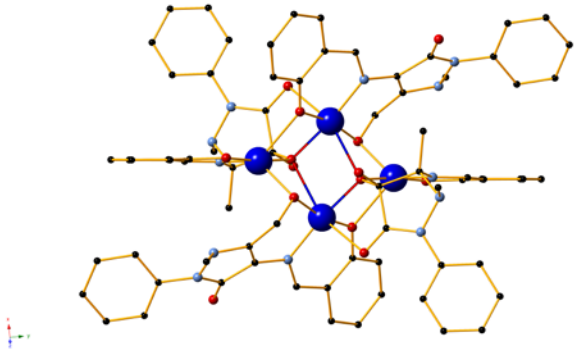

Figure 6. The structure of tetranuclear compound **9**. Colour code Cu (dark blue), O (red), C (black), N (blue). Certain H atoms are omitted for clarity. The axial elongated Cu-O bonds are drawn as double coloured bond.

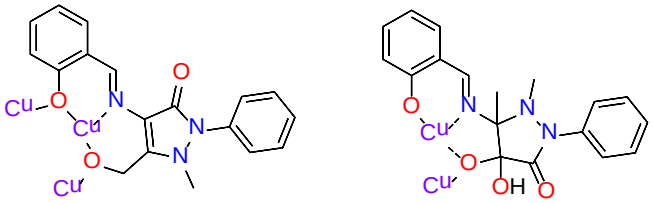

Scheme 3. Coordination modes observed of the transformed ligands in compound **9.**

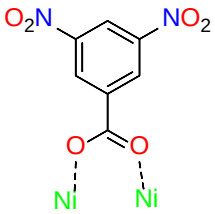

Scheme 4. Coordination mode of the co-ligand in compound **5**

Solution Studies

To confirm their identity in solution, electrospray ionization mass spectrometry (ESI-MS) was also performed for all compounds (Figures S7-S14). The MS (positive-ion mode) for **1** shows two main peaks at the regions of 671.19 and 1034.27 m/z which perfectly correspond to the respective $[Ni(L^1)_2]^+$ and $[Ni_2(L^1)_3]^+$ monocationic fragments. For compounds **3**, **6** and **7** the MS show a main peak at 831.16 m/z that corresponds to the $[M_2(L^1)_2(MeOH)_2 + Na]^+$ monocationic fragment. **3** also shows an additional peak at 944.39 m/z that matches to the $[Cu_2(L^1)_2(piv)_2]^+$ fragment. Complex **4** shows a single peak at 911.15 m/z, which corresponds to the $[Cu_2(L^1)_2(1\text{-nap})]^+$ fragment. The MS for the Ni_2 cluster (complex **5**) has two main peaks, one at 396.08 m/z which corresponds to $[Ni(L^1)(MeOH)]^+$ and a peak at, 892.19 m/z, corresponding to $[Ni_2(L^1)_2(4\text{-nba})]^+$. Compound **8** exhibits two main peaks at 759.14 and 951.66 m/z. These match to the respective $[Ni_2(L^1)_2(CH_3O)]^+$ and $[Ni_5(L^1)_5(CH_3O)_2(OH) - H]^{2+}$ fragments, indicating that the main core remains stable into the solution. Finally, compound **9** has a single peak at 841.15 m/z, corresponding to the $[Cu(L^2)(L^3)(MeCN)_2(H_2O)_2]^+$ monocationic fragment.

Topology Aspects. A survey in Cambridge Structure Database for compounds containing solely five nickel centres yielded 112 entries.[44] Further topological analysis of these compounds using TOPOS software[58] and implementing monoatomic bridges to connect the metal centres[59] yields the following eight motifs shown in Figure 7; two twisted triangles sharing one edge (**2,4M5-1**)[60,61] linear (**1,2,2M5-1**)[62,63], cross-like (**1,4M5-1**)[64,65], trigonal bipyramidal-like (**2,3M5-1**,[66] **2,3,3M5-1**[67] and **3,4M5-1**[68]), ring-like (**2M5-1**)[69,70] and pentagonal like (**4M5-1**)[71]. The topological analysis of compound **8** gives an *ND*k-m symbol **2,3,4M5-1** and this is the first example ever seen in Ni chemistry. Interestingly, the latter topology can be found in compounds containing solely Mn,[72,73] Fe,[74] Co[75–78] and Zn.[79]

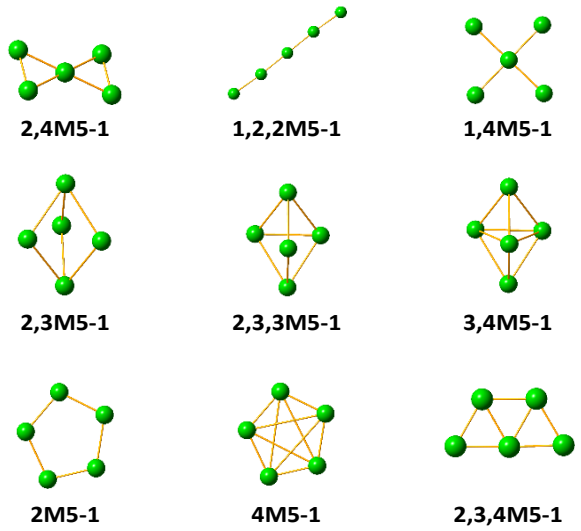

Figure 7. The eight known motifs for Ni_5 chemistry and **2,3,4M5-1** that is found in compound **8**.

Magnetic measurements and modelling

The numbering of the spin carriers in the applied Hamiltonians and in the subsequent discussion for **6 – 9** is provided in Scheme 5. The fit of the experimental data was made for all complexes using PHI program[80] and applying the Hamiltonians derived from the corresponding interaction scheme. Quality of the fits are parametrized as the factor $R = (\chi_M T_{exp} - \chi_M T_{calc})^2/(\chi_M T_{exp})^2$.

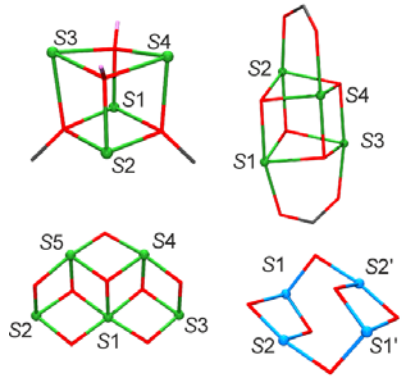

Scheme 5. Schematic draw of cores for compounds **6** (top, left), **7** (top, right), and **8** (bottom left) and **9** (bottom, right) with the numbering of the spin carriers. (see text for the corresponding Hamiltonians).

The room temperature $\chi_M T$ values for the cubane compounds **6** and **7** are 6.06 and 5.45 cm^3 K mol^{-1} respectively. These values are slightly larger than the expected one for four isolated S = 1 local spins. For the two compounds $\chi_M T$ increases continuously up to maximum values of 11.14 cm^3 K mol^{-1} (12 K) and 9.87 cm^3 K mol^{-1} (3 K). Below the maxima $\chi_M T$ value decrease down to 9.03 and 9.42 cm^3 K mol^{-1} at 2 K, Figure 8. The shape of the plots indicates ferromagnetic coupling and S = 4 ground states, as confirm the magnetization experiments that show saturated values of magnetization of 9.13 $N\mu_B$ for **6** and 8.80 $N\mu_B$ for **7**.
The core of complex **6** shows different bond parameters in each one of their six faces. Four of them are contains one phenoxo and one hydroxo bridges whereas two opposite faces exhibit only hydroxo or phenoxo bridges between the Ni^{II} cations. Taking into account that the FM/AF border for these bridges are not the same, the simplified Hamiltonian to fit the experimental data was built attending the kind of bridges as:
$H = -2J_1(S_1 \cdot S_2) - 2J_2(S_3 \cdot S_4) - 2J_3(S_1 \cdot S_3 + S_1 \cdot S_4 + S_2 \cdot S_3 + S_2 \cdot S_4)$
The best fit parameters were J_1 = +5.8 cm^{-1}, J_2 = -5.2 cm^{-1}, J_3 = +6.2 cm^{-1} and g = 2.33, with $R = 1.60 \cdot 10^{-4}$. The FM/AF border for O-hydroxo bridges is placed around 95° and close to 100° for O-phenoxo bridges. In good agreement, J_2 is negative for the face with hydroxo bridges and Ni-O-Ni bond angles larger than 100° whereas J_1 is weakly FM.

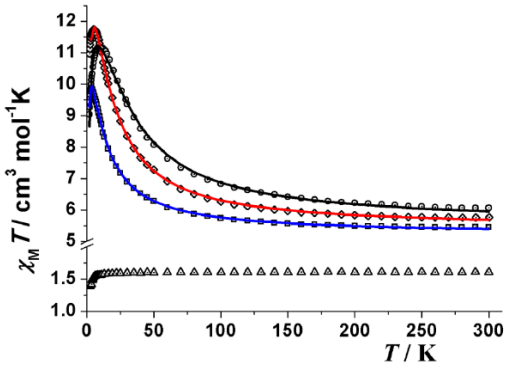

Figure 8. χMT vs. T plot for complexes **6** (circles) **7** (squares), **8** (diamonds) and **9** (triangles). Solid lines show the best obtained fits for **6** and **7** and one of the fits for **8** (see text).

Complex **7** is more symmetric than **6**, showing four similar faces and two opposite faces with an additional carboxylate bridge that forces lower Ni-O-Ni bond angles. In light of the structural data the simplified Hamiltonian was.
$H = -2J_1(S_1 \cdot S_3 + S_2 \cdot S_4) - 2J_2(S_1 \cdot S_2 + S_1 \cdot S_4 + S_2 \cdot S_3 + S_3 \cdot S_4)$
The best fit parameters were J_1 = +6.3 cm^{-1}, J_2 = +0.9 cm^{-1} and g = 2.28, with $R = 3.20 \cdot 10^{-5}$. As in the above case, the low Ni-O-Ni bond angles or around 90° for the two opposite faces parametrized by J_1 becomes clearly FM.

The pentanuclear complex **8** shows a room temperature $\chi_M T$ value of 5.76 cm^3 K mol^{-1} that increases on cooling up to a maximum value of 11.74 cm^3 K mol^{-1} at 5 K indicating a moderate dominant ferromagnetic interaction. The core of this complex is fully asymmetric either by the bond parameters as the μ_3-O bridging ligands (hydroxo or methoxo) and according to Scheme 5 there are seven different interactions that according to the Ni-O-Ni bond angles should be placed around the FM/AF border. Fits performed with different Hamiltonians, joining several interactions under a variety of criteria (bond parameters or kind of ligands) shows that multiple solutions with excellent agreement can be found. The Ni-O-Ni bond angles from the phenoxo bridges are similar (ranging between 95.4-96.7º) as well the Ni-O-Ni bond angles from the μ_3-O donors (ranging from 97.4-100.5º). The simplest fit assuming the same J value for the seven interactions gave a poor fit indicating that all superexchange pathways are not equivalent.

The most obvious difference corresponds to the μ_3-O and μ_3-OMe bridges and thus, fit of the data was tried with the Hamiltonian:

$H = -2J_1(S_1S_2 + S_1S_5 + S_2S_5 + S_4S_5) - 2J_2(S_1S_3 + S_1S_4 + S_3S_4)$

An excellent fit was obtained for J_1 = +4.6 cm^{-1}, J_2 = +0.3 cm^{-1}, g = 2.09 and an intercluster z'J' interaction of -0.02 cm^{-1}, Figure 8. The trial to differentiate the interaction between S_1S_4 and S_1S_3/S_3S_4 gave a similar fit and J values. Absolute values are not fully reliable because the $\chi_M T$ decay at low temperature has been simulated with a zJ' term instead the zero field splitting (D) parameter but the obtained results suggest clearly larger interaction mediated by the methoxo bridges. Magnetization measurements performed up to a field of 5 T show a quasi-saturated value of 8.6 $N\mu_\beta$ which are in agreement with a S = 5 ground state with a magnetization value lower than ten electrons due to the D effect.

Finally, complex **9** shows a practically constant $\chi_M T$ value of 1.60 cm^3 K mol^{-1} indicating a negligible interaction between the Cu^{II} atoms. This feature can be justified by the moderate Cu-O-Cu bond angles and more important, the strong distortion on the coordination sphere of Cu2, intermediate between square pyramidal and trigonal bipyramid, that reduces the effective overlap between the paramagnetic centres.

The $L^1 \rightarrow L^2$ and $L^1 \rightarrow L^3$ ligand transformations in $[Cu_2(L^1)_2]^{2+}$ complexes from a DFT point of view

To probe the $L^1 \rightarrow L^2$ and $L^1 \rightarrow L^3$ ligand transformations taking place in the binuclear $[Cu_2(L^1)_2]^{2+}$ complex yielding the $[Cu_2(L^1)(L^2)]^+$ and $[Cu_2(L^2)(L^3)]$ complexes respectively, the reaction trajectory was explored through DFT calculations of the singlet and triplet PESs along the reaction coordinates and

monitoring the geometric and energetic reaction profile. All calculations were performed using the Gaussian09, D.01 program suite.[82] Computational details with relevant citations are given in the SI. The geometric and energetic reaction profile along the triplet PES is depicted schematically in Figure 9, while the geometric and energetic reaction profile along the singlet PES is given in the SI (Figure S16). It should be noticed that the $[Cu_2(L^1)_2]^{2+}$ complex adopts the triplet as the ground state with the singlet state found 13.4 kcal/mol higher in energy. Each copper(II) metal center in the binuclear $[Cu_2(L^1)_2]^{2+}$ complex is three-coordinate having a T-shaped coordination geometry in both the triplet ground and singlet excited states. The Cu-N_{imine} distances in the triplet state of $[Cu_2(L^1)_2]^{2+}$ are 1.873 and 1.876 Å, and in the singlet state 1.892 and 1.901 Å. The Cu(μ-O)$_2$Cu structural element adopts a distorted rhombic configuration in both the triplet and singlet states with Cu-O-Cu bond angles 96.0 and 98.8° and Cu···Cu distances 2.917 and 3.046 Å respectively. Both Cu···Cu distances exceeding the sum of the copper van der Waals radii (2.80 Å) do not support even weak Cu···Cu interactions. The bridging Cu–O bonds are slightly asymmetric in the triplet state, one with 1.930(3) Å, while the other is 1.990 (1) Å. In the singlet state all bridging Cu-O bonds are asymmetric having bond lengths 1.907, 2.100 Å and 1.926, 2.062 Å.

In a first step, the binuclear $[Cu_2(L^1)_2]^{2+}$ complex interacts with dioxygen yielding the $[Cu_2(L^1)_2(\eta^2\text{-}O_2)]^{2+}$ complex with dioxygen coordinated to Cu(II) metal center in a η^2-coordination mode. The formation of the $[Cu_2(L^1)_2(\eta^2\text{-}O_2)]^{2+}$ complex on the triplet and singlet PESs corresponds to endothermic processes, the estimated Δ*H* values are 12.4 and 14.1 kcal/mol respectively. The natural atomic charges along with the 3D plots of the spin density distribution of all stationary points located on the triplet PES are given in the SI (Figure S17).

An inspection of Figures 9 and S16 reveals that the triplet and singlet states of the binuclear $[Cu_2(L^1)_2]^{2+}$ complex binds O_2 in an asymmetric side-on η^2-O_2 fashion. In the triplet state the O-O bond length is 1.285 Å, close to the O-O bond length of 1.34 Å for a superoxo O-O group, while in the singlet state the O-O bond length is 1.223 Å. It is worth to be noticed that in 1:1 metal-O_2 complexes both the end-on (η^1-) and side-on (η^2-) bonding modes have been identified so far and the corresponding adducts were defined as superoxo or peroxo complexes respectively based primarily on the X-ray structural data (O-O bond distance) and vibrational spectra (O-O stretching frequency, $\nu_{O\text{-}O}$)[81–84]. In particular, when the O-O bond length is ≈ 1.4 - 1.5 Å and the $\nu_{O\text{-}O}$ ≈ 800 - 930 cm^{-1} the compounds are designated as peroxides, whereas when O-O ≈ 1.2–1.3 Å and $\nu_{O\text{-}O}$ ≈ 1050–1200 cm^{-1} the compounds are characterized as superoxides. In the triplet and singlet states of the $[Cu_2(L^1)_2(\eta^2\text{-}O_2)]^{2+}$ complex the O-O bond lengths and the unscalled $\nu_{O\text{-}O}$ stretching vibrational frequencies of 1295 cm^{-1} and 1169 cm^{-1} illustrate the superoxo character of the coordinated η^2-O_2 ligand. The superoxo character of the coordinated η^2-O_2 ligand in the $[Cu_2(L^1)_2(\eta^2\text{-}O_2)]^{2+}$ complex was further corroborated by the spin density distribution of 0.751 and 0.741 au on the two oxygen atoms (Figure S17). Noteworthy, only the copper metal center where the dioxygen is coordinated acquires 0.395 au of spin density. The estimated Cu-O bond distances in the triplet state of the $[Cu_2(L^1)_2(\eta^2\text{-}O_2)]^{2+}$ complex are 1.982 and 2.005 Å, while in the singlet state are 2.137 and 2.652 Å indicating the stronger bonding interactions between $[Cu_2(L^1)_2]^{2+}$ and dioxygen in the triplet state. The η^2-O_2 coordination result in the elongation of the O-O bond by 0.08 and 0.02 Å in the triplet and singlet states respectively. The calculated Cu-N_{imine} distances in the triplet state of $[Cu_2(L^1)_2(\eta^2\text{-}O_2)]^{2+}$ are 1.846 and 1.962 Å, while in the singlet state are 1.873 and 2.009 Å.

The coordinated superoxo radical abstracts a hydrogen atom through a homolytic C-H bond cleavage (*H· transfer*) supported by non covalent (mainly electrostatic) interactions between the negatively charged O atoms of the superoxo group bearing natural atomic charges of -0.159 and -0172 |e| and a hydrogen atom of the methyl substituent which bears positive natural atomic charge of 0.295 |e| (Figure S17) affording a hydroperoxyl ·OOH radical coordinated to Cu(II) metal center. The non covalent interactions are clearly visualized in the Reduced Density Gradient (*RDG*) shown in Scheme 6. An intramolecular electrophilic attack of the C atom of the -CH_3 group by the peroxide group is precluded due to the negative natural atomic charge bearing the C atom of the methyl group (-0.766 |e|).

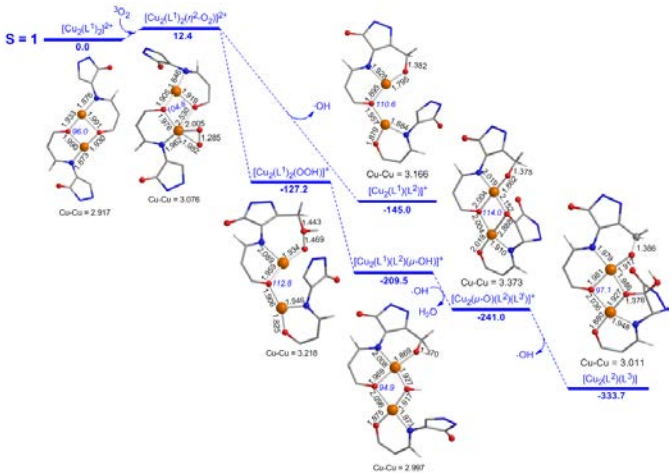

Figure 9. Geometric and energy profile of the reaction trajectory for the $L^1 \rightarrow L^2$ and $L^1 \rightarrow L^3$ ligand transformations in the dinuclear $[Cu_2(L^1)_2]^{2+}$ complex along the triplet PES calculated by the PBE0/Def2-TZVP(Co) ⌣ 6-31G(d,p)(E)/PCM computational protocol in acetonitrile solution.

Homolytic cleavage of the O-O bond in the Cu^{II}-OOH species affords hydroxyl OH radicals with concomitant transformation of the L^1 to L^2 yielding the $[Cu_2(L^1)(L^2)]^+$ complex (Figure 9). The formation of the $[Cu_2(L^1)(L^2)]^+$ complex on both the triplet and singlet PESs is exothermic with estimated Δ*H* values of -132.6 and 130.0 kcal/mol respectively. It should be noticed that the triplet ground state of $[Cu_2(L^1)(L^2)]^+$ complex is more stable than the singlet state by 17.5 kcal/mol. Noteworthy in the singlet state the Cu-Cu distance of 2.493 Å is indicative for remarkable intermetallic interactions, which do not exist in the triplet state having Cu-Cu distance of 3.166 Å.

Alternatively the $[Cu_2(L^1)_2(\eta^2\text{-}O_2)]^{2+}$ complex could be converted to a $[Cu_2(L^1)_2(OOH)]^+$ intermediate with the

coordinated ·OOH radical interacting with the methylenic C atom forming a O-C bond with bond distance of 1.443 Å, while the O-O and Cu-O bond distances are 1.469 and 1.934 Å respectively. These rearrangements correspond also to exothermic processes the estimated Δ*H* values are -114.8 and -126.1 kcal/mol for the triplet and singlet PESs respectively. The $[Cu_2(L^1)_2(OOH)]^+$ intermediate adopting the doublet as the ground state on both the triplet and singlet PESs undergoes further intramolecular rearrangements affording the more stable $[Cu_2(L^1)(L^2)(\mu\text{-OH})]^+$ intermediate which involves the L^2 ligand and a bridging μ-OH bond. The $[Cu_2(L^1)_2(OOH)]^+ \rightarrow [Cu_2(L^1)(L^2)(\mu\text{-OH})]^+$ transformation is predicted to be exothermic, the estimated exothermicity being -82.3 kcal/mol.

Next hydroxyl radical interacts with the $[Cu_2(L^1)(L^2)(\mu\text{-OH})]^+$ intermediate transforming the L^1 to $L^{3'}$ ligand with concomitant release of a water molecule affording the $[Cu_2(\mu\text{-O})(L^{3'})(L^2)]$ intermediate through an exothermic process with estimated Δ*H* values of -31.5 and -21.8 kcal/mol for the triplet and singlet PESs respectively. Further reaction of the $[Cu_2(\mu\text{-O})(L^{3'})(L^2)]$ intermediate with hydroxyl radicals affords the $[Cu_2(L^3)(L^2)]$ product, thus completing the $L^1 \rightarrow L^3$ transformation. The triplet states of the $[Cu_2(\mu\text{-O})(L^{3'})(L^2)]$ intermediate and $Cu_2(L^3)(L^2)]$ product are more stable than the singlet states by 12.2 and 33.6 kcal/mol respectively. The mean Cu-O bond distances in the triplet state of the $[Cu_2(L^3)(L^2)]$ product range from 1.880 to 2.036 Å in good agreement with experiment. As in the case of the solid state structure of the $[Cu_2(L^3)(L^2)]_2$ product a hydrogen bond is formed between the protonated hydroxyl group of $[HL^3]^{2-}$ and the deprotonated transformed hydroxy group of $[HL^3]^{2-}$ with a OH ··· O bond distance of 2.304 Å.

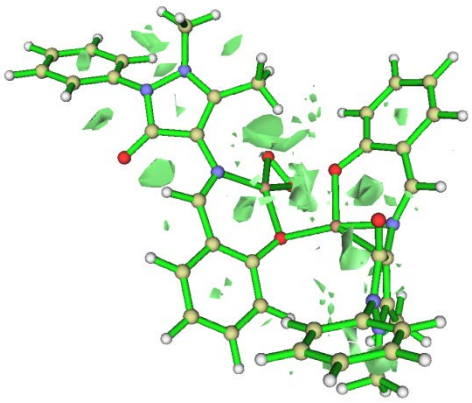

Scheme 6. 3D plot of the Reduced Density Gradient (*RDG* = 0.75 au) for the $[Cu_2(L^1)_2(\eta^2\text{-}O_2)]^{2+}$ complex.

Conclusions

The first examples of polynuclear 3d CCs constructed from (E)-4-(2-hydroxybenzylideneamino)-2,3-dimethyl-1-phenyl-1,2-dihydropyrazol-5-one (HL^1) Schiff base ligand are reported in this study. The use of a variety of co-ligands influence the final topology and nuclearity, whereas the use of redox active metals (i.e. Cu) may yield to oxidation of the main organic scaffold. The present synthetic strategy highlights are i) a pentanuclear CC Ni_5 (**8**); its topology has never been seen in Ni chemistry and ii) a tetranuclear CC Cu_4 in which an interesting ligand transformation, involving atmospheric oxygen absorption, has occurred. The $L^1 \rightarrow L^2$ and $L^1 \rightarrow L^3$ ligand transformations taking place in a binuclear $[Cu_2(L^1)_2]^{2+}$ complex yielding stepwise the $[Cu_2(L^1)(L^2)]^+$ and $[Cu_2(L^2)(L^3)]$ complexes respectively. These findidings are probed by DFT calculations of the singlet and triplet PESs along the reaction trajectories and monitoring the geometric and energetic reaction profile. The present work illustrates that the proposed methodology represents an effective synthetic tool to construct high nuclearity CCs with unseen topologies as well molecular models to understand the bio-activity of ampyrone (cycotoxic, antimicrobial, analgesic). Ongoing investigations for the synthesis of other derivatives are in progress in our laboratory.

Conflicts of interest

There are no conflicts to declare

Acknowledgements

We thank the EPSRC UK National Crystallography Service at the University of Southampton[26] for the collection of the crystallographic data for compounds **3**, **4** and **9**. AE thanks founds from Ministerio de Economia y Competitividad, Project CTQ2015-63614-P.

References

1. L. Cronin and J. Fielden, in *Coordination Clusters in Encyclopedia of Supramolecular Chemistry, Taylor and Francis, London, 2007,* Taylor & Francis, 2007, pp. 1–10.
2. C. Zhang, C. Chen, H. Dong, J.-R. Shen, H. Dau, and J. Zhao, *Science*, 2015, **348**, 690–693.
3. J. S. Kanady, E. Y. Tsui, M. W. Day, and T. Agapie, *Science*, 2011, **333**, 733–736.
4. S. Muche, I. Levacheva, O. Samsonova, L. Pham, G. Christou, U. Bakowsky, and M. Hołyńska, *Inorg. Chem.*, 2014, **53**, 7642–7649.
5. M. Hołyńska, R. Clérac, and M. Rouzières, *Chem. Eur. J.*, 2015, **21**, 13321–13329.
6. I. A. Kühne, V. Mereacre, C. E. Anson, and A. K. Powell, *Chem. Commun.*, 2016, **52**, 1021–1024.
7. S. Chen, V. Mereacre, C. E. Anson, and A. K. Powell, *Dalton Trans.*, 2016, **45**, 9336–9344.
8. S. Schmitz, J. van Leusen, A. Ellern, P. Kögerler, and K. Y. Monakhov, *Inorg. Chem. Front.*, 2016, **3**, 523–531.
9. F. Gai, X. Li, T. Zhou, X. Zhao, D. Lu, Y. Liu, and Q. Huo, *J. Mater. Chem. B*, 2014, **2**, 6306–6312.
10. C. Y. Chow, S. V Eliseeva, E. R. Trivedi, T. N. Nguyen, J. W. Kampf, S. Petoud, and V. L. Pecoraro, *J. Am. Chem. Soc.*, 2016, **138**, 5100–9.
11. J. Jankolovits, C. M. Andolina, J. W. Kampf, K. N. Raymond, and V. L. Pecoraro, *Angew. Chem. Int. Ed.*, 2011, **50**, 9660–9664.
12. J. Long, J. Rouquette, J.-M. Thibaud, R. A. S. Ferreira, L. D. Carlos, B. Donnadieu, V. Vieru, L. F. Chibotaru, L. Konczewicz, J. Haines, Y. Guari, and J. Larionova, *Angew. Chem. Int. Ed.*, 2015, **54**, 2236–2240.
13. X.-Q. Song, P.-P. Liu, Y.-A. Liu, J.-J. Zhou, and X.-L. Wang, *Dalton Trans.*, 2016, **45**, 8154–8163.
14. G. Guthausen, J. R. Machado, B. Luy, A. Baniodeh, A. K. Powell, S. Krämer, F. Ranzinger, M. P. Herrling, S. Lackner, and H. Horn, *Dalton Trans.*, 2015, **44**, 5032–5040.

15. A. Baniodeh, Y. Liang, C. E. Anson, N. Magnani, A. K. Powell, A.-N. Unterreiner, S. Seyfferle, M. Slota, M. Dressel, L. Bogani, and K. Goß, *Adv. Funct. Mater.*, 2014, **24**, 6280–6290.
16. K.-H. Chang, C.-C. Huang, Y.-H. Liu, Y.-H. Hu, P.-T. Chou, and Y.-C. Lin, *Dalton Trans.*, 2004, 1731–1738.
17. H.-C. Lin, C.-C. Huang, C.-H. Shi, Y.-H. Liao, C.-C. Chen, Y.-C. Lin, and Y.-H. Liu, *Dalton Trans.*, 2007, 781–791.
18. K. S. Rathore, B. S. Lad, H. Chennamsetti, and S. Katukojvala, *Chem. Commun.*, 2016, **52**, 5812–5815.
19. A. N. Bilyachenko, M. S. Dronova, A. I. Yalymov, F. Lamaty, X. Bantreil, J. Martinez, C. Bizet, L. S. Shul'pina, A. A. Korlyukov, D. E. Arkhipov, M. M. Levitsky, E. S. Shubina, A. M. Kirillov, and G. B. Shul'pin, *Chem. Eur. J.*, 2015, **21**, 8758–8770.
20. S. S. P. Dias, M. V Kirillova, V. André, J. Kłak, and A. M. Kirillov, *Inorg. Chem.*, 2015, **54**, 5204–5212.
21. R. E. P. Winpenny, *J. Chem. Soc. Dalt. Trans.*, 2002, 1–10.
22. B. Gole, K. C. Mondal, and P. S. Mukherjee, *Inorg. Chim. Acta*, 2014, **415**, 151–164.
23. P. S. Perlepe, L. Cunha-Silva, K. J. Gagnon, S. J. Teat, C. Lampropoulos, A. Escuer, and T. C. Stamatatos, *Inorg. Chem.*, 2016, **55**, 1270–1277.
24. E. C. Mazarakioti, K. M. Poole, L. Cunha-Silva, G. Christou, and T. C. Stamatatos, *Dalt. Trans.*, 2014, **43**, 11456–11460.
25. L. Zhao, J. Wu, H. Ke, and J. Tang, *Inorg. Chem.*, 2014, **53**, 3519–3525.
26. Y. Deng, L. Liu, R. G. Sarkisian, K. Wheeler, H. Wang, and Z. Xu, *Angew. Chem. Int. Ed.*, 2013, **52**, 3663–3667.
27. M. Machata, I. Nemec, R. Herchel, and Z. Trávníček, *RSC Adv.*, 2017, **7**, 25821–25827.
28. R. Herchel, I. Nemec, M. Machata, and Z. Trávníček, *Dalt. Trans.*, 2016, **45**, 18622–18634.
29. F.-V. Lauro, D.-C. Francisco, G.-C. Elodia, P.-G. Eduardo, R.-N. Marcela, H.-H. Lenin, and S. A. Betty, *Steroids*, 2015, **95**, 39–50.
30. Premnath, M. Selvakumar, Ravichandiran, T. Selvan, Indiraleka, and J. Vennila, *Spectrochim. Acta - Part A Mol. Biomol. Spectrosc.*, 2016, **153**, 118–123.
31. El-Sonbati, Diab, El-Bindary, Mohamed, Morgan, Abou-Dobara, and Nozha, *J. Mol. Liq.*, 2016, **215**, 423–442.
32. S. Maione, L. Radanova, D. De Gregorio, L. Luongo, L. De Petrocellis, V. Di Marzo, and P. Imming, *Eur. J. Pharmacol.*, 2015, **748**, 115–122.
33. P. Ali, J. Meshram, J. Sheikh, V. Tiwari, R. Dongre, and T. B. Hadda, *Med. Chem. Res.*, 2012, **21**, 157–164.
34. I. N. Booysen, S. Maikoo, M. P. Akerman, and B. Xulu, *Polyhedron*, 2014, **79**, 250–257.
35. P. A. Fatullayeva, A. A. Medjidov, A. M. Maharramov, A. V Gurbanov, R. K. Askerov, K. Q. Rahimov, M. N. Kopylovich, K. T. Mahmudov, and A. J. L. Pombeiro, *Polyhedron*, 2012, **44**, 72–76.
36. J.-S. Wu, J.-H. Zhou, P.-F. Wang, X.-H. Zhang, and S.-K. Wu, *Org. Lett.*, 2005, **7**, 2133–2136.
37. V. Luxami, A. Sen Gupta, and K. Paul, *New J. Chem.*, 2014, **38**, 2841–2846.
38. Y. Li, C. Liao, S. Huang, H. Xu, B. Zheng, J. Du, and D. Xiao, *RSC Adv.*, 2016, **6**, 25420–25426.
39. K. Hunger and W. Herbst, in *Ullmann's Encyclopedia of Industrial Chemistry*, Wiley-VCH Verlag GmbH & Co. KGaA, 2000.
40. E. Loukopoulos, B. Berkoff, A. Abdul-Sada, G. J. Tizzard, S. J. Coles, A. Escuer, and G. E. Kostakis, *Eur. J. Inorg. Chem.*, 2015, **2015**, 2646–2649.
41. B. Berkoff, K. Griffiths, A. Abdul-Sada, G. J. Tizzard, S. J. Coles, A. Escuer, and G. E. Kostakis, *Dalton Trans.*, 2015, **44**, 12788–12795.
42. E. Loukopoulos, B. Berkoff, K. Griffiths, V. Keeble, V. N. Dokorou, A. C. Tsipis, A. Escuer, and G. E. Kostakis, *CrystEngComm*, 2015, **17**, 6753–6764.
43. K. Griffiths, C. Harding, V. N. Dokorou, E. Loukopoulos, S. I. Sampani, A. Abdul-Sada, G. J. Tizzard, S. J. Coles, G. Lorusso, M. Evangelisti, A. Escuer, and G. E. Kostakis, *Eur. J. Inorg. Chem.*, 2017, **2017**, 3938–3945.
44. F. H. Allen, *Acta Crystallogr. Sect. B-Structural Sci.*, 2002, **58**, 380–388.
45. T. Rosu, E. Pahontu, C. Maxim, R. Georgescu, N. Stanica, and A. Gulea, *Polyhedron*, 2011, **30**, 154–162.
46. P. M. Selvakumar, Suresh, and Subramanian, *Polyhedron*, 2007, **26**, 749–756.
47. K. C. Potgieter, T. I. A. Gerber, and P. Mayer, *South African J. Chem.*, 2011, **64**, 179–184.
48. R. M. El-Mehdawi, A. N. Eldewik, K. M. Kreddan, S. H. El-Hamruni, H. B. Hussien, P. B. Hitchcock, and A. A. Shabash, *Jordan J. Chemisrty*, 2010, **5**, 157–164.
49. X.-W. Wang and Y.-Q. Zheng, *Inorg. Chem. Commun.*, 2007, **10**, 709–712.
50. S. J. Coles and P. A. Gale, *Chem. Sci.*, 2012, **3**, 683–689.
51. O. V Dolomanov, A. J. Blake, N. R. Champness, and M. Schröder, *J. Appl. Crystallogr.*, 2003, **36**, 1283–1284.
52. G. M. Sheldrick, *Acta Crystallogr. Sect. A Found. Adv.*, 2015, **71**, 3–8.
53. G. M. Sheldrick, *Acta Crystallogr. Sect. A*, 2008, **64**, 112–122.
54. A. L. Spek, *J. Appl. Crystallogr.*, 2003, **36**, 7–13.
55. L. J. Farrugia, *J. Appl. Crystallogr.*, 1999, **32**, 837–838.
56. C. F. Macrae, P. R. Edgington, P. McCabe, E. Pidcock, G. P. Shields, R. Taylor, M. Towler, and J. Van De Streek, *J. Appl. Crystallogr.*, 2006, **39**, 453–457.
57. A. W. Addison, T. N. Rao, J. Reedijk, J. van Rijn, and G. C. Verschoor, *J. Chem. Soc., Dalton. Trans.*, 1984, 1349–1356.
58. V. A. Blatov, A. P. Shevchenko, and D. M. Proserpio, *Cryst. Growth Des.*, 2014, **14**, 3576–3586.
59. G. E. Kostakis, V. A. Blatov, and D. M. Proserpio, *Dalton Trans.*, 2012, **41**, 4634–4640.
60. A. J. Finney, M. A. Hitchman, C. L. Raston, G. L. Rowbottom, and A. H. White, *Aust. J. Chem.*, 1981, **34**, 2139–2157.
61. C. Papatriantafyllopoulou, T. C. Stamatatos, W. Wernsdorfer, S. J. Teat, A. J. Tasiopoulos, A. Escuer, and S. P. Perlepes, *Inorg. Chem.*, 2010, **49**, 10486–10496.
62. C. C. Wang, W. C. Lo, C. C. Chou, G. H. Lee, J. M. Chen, and S. M. Peng, *Inorg. Chem.*, 1998, **37**, 4059–4065.
63. A. K. Boudalis, M. Pissas, C. P. Raptopoulou, V. Psycharis, B. Abarca, and R. Ballesteros, *Inorg. Chem.*, 2008, **47**, 10674–10681.
64. G. Psomas, A. J. Stemmler, C. Dendrinou-Samara, J. J. Bodwin, M. Schneider, M. Alexiou, J. W. Kampf, D. P. Kessissoglou, and V. L. Pecoraro, *Inorg. Chem.*, 2001, **40**, 1562–1570.
65. Z. Chen, M. Jia, Z. Zhang, and F. Liang, *Cryst. Growth Des.*, 2010, **10**, 4806–4814.
66. S. Feng, M. Zhu, L. Lu, L. Du, Y. Zhang, and T. Wang, *Dalton Trans.*, 2009, 6385–6395.
67. Y.-L. Zhou, F.-Y. Meng, J. Zhang, M.-H. Zeng, and H. Liang, *Cryst. Growth Des.*, 2009, **9**, 1402–1410.
68. R. Ahlrichs, D. Fenske, H. Oesen, and U. Schneider, *Angew. Chem. Int. Ed.*, 1992, **31**, 323–326.
69. A. H. Mahmoudkhani and V. Langer, *Inorg. Chim. Acta*, 1999, **294**, 83–86.
70. T. C. Stamatatos, E. Diamantopoulou, C. P. Raptopoulou, V. Psycharis, A. Escuer, and S. P. Perlepes, *Inorg. Chem.*, 2007, **46**, 2350–2352.
71. O. L. Sydora, P. T. Wolczanski, E. B. Lobkovsky, E. Rumberger, and D. N. Hendrickson, *Chem. Commun.*, 2004, 650–651.
72. M. Wang, C.-B. Ma, D.-Q. Yuan, H.-S. Wang, C.-N. Chen, and Q.-T. Liu, *Inorg. Chem.*, 2008, **47**, 5580–5590.
73. C. Kozoni, M. Siczek, T. Lis, E. K. Brechin, and C. J. Milios, *Dalton Trans.*, 2009, **38**, 9117–9119.
74. G. Fischer, G. Sedelmeier, H. Prinzbach, K. Knoll, P. Wilharm, G. Huttner, and I. Jibril, *J. Organomet. Chem.*, 1985, **297**, 307–312.
75. B. T. Zhuang, P. H. Yu, L. G. Huang, L. J. He, and G. H. Pan, *Polyhedron*, 1997, **16**, 1425–1431.
76. G. Aromi, A. S. Batsanov, P. Christian, M. Helliwell, A. Parkin, S. Parsons, A. A. Smith, G. A. Timco, and R. E. P. Winpenny, *Chem. Eur. J.*, 2003, **9**, 5142–5161.

77. A. Ferguson, M. Schmidtmann, E. K. Brechin, and M. Murrie, *Dalton Trans.*, 2011, **40**, 334–336.
78. L.-L. Hu, Z.-Q. Jia, J. Tao, R.-B. Huang, and L.-S. Zheng, *Dalton Trans.*, 2008, **365**, 6113–6116.
79. N. Hollingsworth, A. L. Johnson, A. Kingsley, G. Kociok-Köhn, and K. C. Molloy, *Organometallics*, 2010, **29**, 3318–3326.
80. N. F. Chilton, R. P. Anderson, L. D. Turner, A. Soncini, and K. S. Murray, *J. Comput. Chem.*, 2013, **34**, 1164–1175.
81. M. H. Gubelmann and A. F. Williams, *Struct. Bond.*, 1983, **55**, 2–65.
82. C. J. Cramer, W. B. Tolman, K. H. Theopold, and A. L. Rheingold, *Proc. Natl. Acad. Sci. U. S. A.*, 2003, **100**, 3635–3640.
83. J. W. Egan, B. S. Haggerty, A. L. Rheingold, S. C. Sendlinger, and K. H. Theopold, *J. Am. Chem. Soc.*, 1990, **112**, 2445–2446.
84. A. Hess, M. R. Hörz, L. M. Liable-Sands, D. C. Lindner, A. L. Rheingold, and K. H. Theopold, *Angew. Chemie Int. Ed.*, 1999, **38**, 166–168.